REUSABLE LAUNCH VEHICLE CONTROL IN MULTIPLE TIME SCALE SLIDING MODES

Yuri Shtessel

Department of Electrical and Computer Engineering, University of Alabama in Huntsville, Huntsville, Alabama 35899

Charles Hall, and Mark Jackson

TD55, Vehicle and Systems Development, NASA Marshall Space Flight Center, MSFC, Alabama 35812

Abstract

A reusable launch vehicle control problem during ascent is addressed via multiple-time scaled continuous sliding mode control. The proposed sliding mode controller utilizes a two-loop structure and provides robust, de-coupled tracking of both orientation angle command profiles and angular rate command profiles in the presence of bounded external disturbances and plant uncertainties. Sliding mode control causes the angular rate and orientation angle tracking error dynamics to be constrained to linear, de-coupled, homogeneous, and vector valued differential equations with desired eigenvalues placement. Overall stability of a two-loop control system is addressed. An optimal control allocation algorithm is designed that allocates torque commands into end-effector deflection commands, which are executed by the actuators. The dual-time scale sliding mode controller was designed for the X-33 technology demonstration sub-orbital launch vehicle in the launch mode. Simulation results show that the designed controller provides robust, accurate, de-coupled tracking of the orientation angle command profiles in presence of external disturbances and vehicle inertia uncertainties. This is a significant advancement in performance over that achieved with linear, gain scheduled control systems currently being used for launch vehicles.

Introduction

Flight control of both current and future reusable launch vehicles (RLV) in ascent mode involves attitude maneuvering through a wide range of flight conditions, wind disturbances, and plant uncertainties. A flight control algorithm that is robust to changing flight conditions, disturbances, and vehicle uncertainties would be an improvement over current RVL flight control technology. Sliding Mode Controller (SMC) is an attractive robust control algorithm for RLV ascent designs because of its inherent insensitivity and robustness to plant uncertainties and external disturbances[1-3].

A SMC design consists of two major steps: (1) a sliding surface is designed such that the system motion on this surface exhibits desired behavior in the presence of plant uncertainties and disturbances; and (2) a control function is designed that causes the system state to reach the sliding surface in finite time and guarantees system motion in this surface thereafter. The system's motion on the sliding surface is called sliding mode. Strict enforcement of the sliding mode typically leads to discontinuous control functions and possible control chattering effects[4]. Control chattering is typically an unwanted effect that is easily eliminated by continuous approximations of discontinuous control functions[4,5], or by continuous SMC designs[6].

An example of the application of SMC is shown in the spacecraft attitude control work performed by Dwyer et al[7]. This work utilizes the natural time-scale separation, which exists in the system dynamics of many aerospace control problems[8].

The RLV SMC architecture, which is developed in this paper, is a two loop structure[9] that incorporates backstepping techniques[10]. In the outer loop, the kinematics equation of angular motion is used with the outer loop SMC to generate the angular rate profiles as virtual control inputs to the inner loop. In the inner loop, a suitable inner loop SMC is designed so that the

commanded angular rate profiles are tracked. The inner loop SMC produces roll, pitch and yaw torque commands, which are optimally allocated into end-effector deflection commands. Multiple time scaling (multiple-scale) is defined as the time-constant separation between the two loops. That is, the inner loop compensated dynamics is designed to be faster than the outer loop dynamics. The resulting multiple-scale two-loop SMC, with optimal torque allocation, causes the angular rate and the Euler angle tracking errors to be constrained to linear de-coupled homogeneous vector valued differential equations with desired eigenvalues placement.

Simulation results are presented that demonstrate the SMC's effectiveness in causing the X-33 technology demonstration Launch vehicle, operating in ascent mode, to robustly follow the desired profiles. The resulting design controls large attitude maneuvers through a wide range of flight conditions, provides highly accurate tracking of guidance trajectories, and exhibits robustness to external disturbances and parametric uncertainties.

Equations of RLV dynamics

The dynamic equations of rotational motion of the rigid-body RLV are given by the Euler equation in the body frame

$$(\mathbf{J}_0 + \Delta\mathbf{J})\dot{\omega} = -\Omega(\mathbf{J}_0 + \Delta\mathbf{J})\omega + \mathbf{T} + \mathbf{d} \ , \tag{1}$$

where $\mathbf{J}_0 \in \mathbf{R}^{3\times3}$ is the nominal inertia matrix, $\Delta\mathbf{J} \in \mathbf{R}^{3\times3}$ is an uncertain part of the inertia matrix, caused by fuel consumption and variations of particular payloads from a nominal one, $\omega = [p \quad q \quad r]^T$ is the angular rate vector, $\mathbf{T} = \{L, M, N\}^T$ is the control torque vector, $\mathbf{d} = \{L_d, M_d, N_d\}^T$ is the external disturbance torque vector. The matrix Ω is given by:

$$\Omega = \begin{bmatrix} 0 & -\omega_3 & \omega_2 \\ \omega_3 & 0 & -\omega_1 \\ -\omega_2 & \omega_1 & 0 \end{bmatrix}. \tag{2}$$

The RLV orientation dynamics are described by the kinematics equation on the body axes

$$\dot{\gamma} = \mathbf{R}(\gamma)\omega, \tag{3}$$

where

$$\begin{cases} \mathbf{R}(\gamma) = \begin{bmatrix} 1 & \tan\theta\sin\varphi & \tan\theta\cos\varphi \\ 0 & \cos\varphi & -\sin\varphi \\ 0 & \dfrac{\sin\varphi}{\cos\theta} & \dfrac{\cos\varphi}{\cos\theta} \end{bmatrix} \\ \gamma = [\varphi \quad \theta \quad \psi]^T \end{cases}. \tag{4}$$

The RLV equations of the translational motion are given in the body frame as

$$\dot{\mathbf{v}} = H\omega - g\Phi + \frac{1}{M}\mathbf{F} \tag{5}$$

where

$$H = \begin{bmatrix} 0 & -v_z & v_y \\ v_z & 0 & -v_x \\ -v_y & v_x & 0 \end{bmatrix}, \tag{6}$$

$\mathbf{v} = [v_x, v_y, v_z]^T$ is the linear velocity vector, M is the mass of RLV, $\mathbf{F}$ is the vector of external forces acting on RLV, $\Phi = [\sin\varphi \quad \cos\theta\sin\varphi \quad \cos\theta\cos\varphi]^T$, and $g = 9.81 m/s^2$ is a gravitational constant. The total mass expenditure onboard the RLV in the launch mode is described as follows:

$$M = m_{dry} + m_f, \quad m_f = m_{f0} - \dot{m}_f t, \quad \dot{m}_f = \begin{cases} \dot{m}_0, & if\ m_f > 0 \\ 0, & if\ m_f = 0 \end{cases}, \tag{7}$$

where m_f and m_{f0} are the current and initial fuel masses, respectively, m_{dry} is a mass of the RLV without fuel (dry), and $\dot{m}_f$ is a rate of fuel consumption.

The control torque $\mathbf{T}$ is generated by the aerodynamic surfaces and rocket engines. This is described by the equation

$$\mathbf{T} = \mathbf{D}(.)\delta , \tag{8}$$

where $\mathbf{D}(.) \in \mathbf{R}^{3\times n}$ is a sensitivity matrix calculated on the basis of table lookup data, $\delta \in \mathbf{R}^n$ is the vector of aerodynamic surface deflections and differential throttles of the rocket engines.

Electromechanical actuators deflect the aerodynamic surfaces (aerosurfaces), and thrust-vector-control valves that throttle the rocket engines. The actuator dynamics are assumed to be much faster than the dynamics of the compensated RLV flight control system.

Problem Formulation

The general problem formulation is to determine the actuator deflection commands δ_c such that the commanded Euler angle profiles $\gamma_c = [\varphi_c \quad \theta_c \quad \psi_c]^T$ are robustly followed in the presence of bounded disturbance torques $\mathbf{d}$ and plant inertia variations $\Delta\mathbf{J}$. This problem is addressed as follows:

- A control law is designed in terms of the control torque command vector $\mathbf{T}_c$, and
- An optimal control allocation matrix $\mathbf{B}_v$ is designed to map the control torque command vector $\mathbf{T}_c$ to actuator deflection commands. That is,

$$\delta_c = \mathbf{B}_v \mathbf{T}_c . \tag{9}$$

- The "fast" actuator dynamics are neglected at the stage of the controller design. They must be used during simulations to validate the designed controller.

Specifically, the control problem for the RLV in launch mode is to determine the control torque input command vector $\mathbf{T}_c$ in the given state variable equations

$$\begin{cases} (\mathbf{J}_0 + \Delta\mathbf{J})\dot{\omega} = -\Omega(\mathbf{J}_0 + \Delta\mathbf{J})\omega + \mathbf{T}_c + \mathbf{d}, \\ \dot{\gamma} = \mathbf{R}(\gamma)\omega, \\ \mathbf{y} = \gamma \end{cases} \tag{10}$$

such that the output vector $\mathbf{y}$ asymptotically tracks a command orientation angle profile $\mathbf{y}_c = \gamma_c$. That is,

$$\lim_{t\to\infty} \| y_{ic}(t) - y_i(t) \| = 0 \quad \forall i = \overline{1,3}. \tag{11}$$

The desired RLV performance criteria is to robustly track both the commanded Euler angle guidance profiles γ_c and the real-time generated angular rate profiles ω_c, such that the motion for each quantity is described by a linear, de-coupled, and homogeneous vector valued differential equations with given eigenvalues placement.

Sliding Mode Controller Design

Tracking of the commanded Euler angles guidance profile γ_c (the primary objective) is achieved through a two loop SMC structure[9]. The cascade structure of the system in eq. (10) and the inherent two time scale nature of the RLV flight control problem are exploited for design of a two loop flight control system using continuous SMCs in the inner and outer loops. The outer loop SMC provides angular rate commands ω_c to the inner loop. The inner loop SMC provides robust de-coupled tracking of angular rates ω. Together, the inner and outer loop SMCs form a two loop flight control system that achieves de-coupled asymptotic tracking of the command angle guidance profile γ_c. Similar structure was developed[11] for an aircraft control system using a dynamic inversion algorithm.

Outer Loop Sliding Mode Controller Design

The outer loop SMC takes the vehicle's angular rate vector ω as a virtual control ω_c and uses the kinematics eq. (3) to compensate the Euler angle tracking dynamics. The motion of the outer loop compensated tracking error dynamics, with desired bandwidth, is constrained (by proper control action) to a sliding surface of the form

$$\sigma = \gamma_e + \mathbf{K}_1 \int_0^t \gamma_e d\tau, \quad \sigma \in \mathbf{R}^3, \tag{12}$$

where $\gamma_e = \gamma_c - \gamma$ and $\mathbf{K}_1 = diag\{k_{1i}\}$, $\mathbf{K}_1 \in \mathbf{R}^{3\times 3}$. The gain matrix $\mathbf{K}_1$ is chosen so that the output tracking error γ_e exhibits a desired linear asymptotic behavior on the sliding surface ($\sigma = 0$).

The objective of the outer loop SMC is to generate the commanded angular rate vector ω_c (which is passed to the inner loop SMC) necessary to cause the vehicle's trajectory to track the commanded Euler angles guidance profile γ_c. In other words, the virtual control law ω_c is designed to provide asymptotic convergence (with finite reaching time) of the system's eq. (3) trajectory to the sliding surface $\sigma = 0$. Dynamics of the sliding surface in eq. (12) are described as

$$\dot{\sigma} = \dot{\gamma}_c - \mathbf{R}(\gamma)\omega_c + \mathbf{K}_1\gamma_e. \tag{13}$$

The outer loop SMC design is initiated by choosing a candidate Lyapunov function of the form

$$V = \frac{1}{2}\sigma^T\sigma > 0, \tag{14}$$

whose derivative is shown as

$$\dot{V} = \sigma^T\dot{\sigma} = \sigma^T[\dot{\gamma}_c - \mathbf{R}(\gamma)\omega_c + \mathbf{K}_1\gamma_e]. \tag{15}$$

To ensure asymptotic stability of the origin of the system in eq. (13), the following derivative inequality of the candidate Lyapunov function is enforced[1-4]

$$\dot{V} = -\rho\sigma^T SIGN(\sigma) = -\rho\sum_{i=1}^{3}|\sigma_i|, \quad \rho > 0. \tag{16}$$

Considering equality (16), the required angular rate command ω_c to ensure asymptotic stability is defined as

$$\omega_c = \mathbf{R}^{-1}(\gamma)[\dot{\gamma}_c + \mathbf{K}_1\gamma_e] + \mathbf{R}^{-1}(\gamma)\rho SIGN(\sigma), \tag{18}$$

where $SIGN(\sigma) = [sign(\sigma_1), sign(\sigma_2), sign(\sigma_3)]^T$, and $\rho > 0$.

The sliding surface shown in eq. (12) will reach zero in a finite time[1-4] defined as

$$t_r = \max_{i\in[1,3]}\frac{|\sigma_i(0)|}{\rho}, \tag{19}$$

where $\rho > 0$, and t_r is the design parameter describing the sliding surface reaching time. The value of ρ is calculated using inequality (19).

The angular rate command profile in eq. (18) is discontinuous; as a result, the control actuation will chatter during system operation on the sliding surface eq. (12). Mechanically and electrically, this chattering is an unwanted effect. Moreover, a discontinuous profile cannot be accurately tracked in the inner loop. To solve this problem, the discontinuous term ($SIGN(\sigma)$) in eq. (18) is replaced by the high-gain linear term

$$\mathbf{K}_0\sigma = \left\{\frac{\sigma_1}{\varepsilon_1}, \frac{\sigma_2}{\varepsilon_2}, \frac{\sigma_3}{\varepsilon_3}\right\}^T, \mathbf{K}_0 = diag\left\{\frac{1}{\varepsilon_i}\right\} \quad \forall\varepsilon_i > 0 \; \forall\overline{1,3}, \tag{20}$$

where $\varepsilon_i > 0 \; \forall\overline{1,3}$ define the slopes of the linearized function[4,5].

After substitution of eqs. (20) and (18) into eq. (13), the sliding surface dynamics are of the form

$$\dot{\sigma} = -\rho \mathbf{K}_0 \sigma \,. \tag{21}$$

Eq. (21) is globally asymptotically stable, since $\rho > 0$ and $\mathbf{K}_0$ is positive definite, and the equilibrium $\sigma = 0$ will be reached asymptotically. Moreover, in a close vicinity of $\sigma_i = 0$, $\forall i = \overline{1,3}$, the tracking error γ_e will exhibit de-coupled motion in accordance with eq. (14).

Inner Loop Sliding Mode Controller Design

The purpose of the inner loop SMC is to generate the vehicle torque command vector $\mathbf{T}_c$ necessary to track the given commanded angular rate profile ω_c. In addition to solving the inner loop tracking problem defined as

$$\lim_{t\to\infty} \left\| \omega_{ic}(t) - \omega_i(t) \right\| = 0, \ \forall i = 1,3, \tag{22}$$

SMC causes the system to exhibit linear decoupled motion in sliding mode.

The motion of the inner loop compensated dynamics, with desired bandwidth, is constrained (by proper control action) to a sliding surface of the form

$$s = \omega_e + \mathbf{K}_2 \int_0^t \omega_e d\tau \,, \quad s \in \mathbf{R}^3, \tag{23}$$

where $\omega_e = \omega_c - \omega$ and $\mathbf{K}_2 = diag\{k_2\}$, $\mathbf{K}_2 \in \mathbf{R}^{3\times 3}$. The angular rate tracking error ω_e exhibits a desired linear asymptotic behavior while operating on the sliding surface ($s = 0$) and with proper choice of $\mathbf{K}_2$. The inner loop sliding mode dynamics in eq. (23) are designed faster than the outer-loop sliding mode dynamics in eq. (14) in order to preserve sufficient time scale separation between the loops.

The command torque $\mathbf{T}_c$ is designed to provide asymptotic convergence (with finite reaching time) of the system's eq. (1) trajectory to the sliding surface $s = 0$. Dynamics of the sliding surface eq. (23) are described as follows:

$$\dot{s} = \dot{\omega}_c + (\mathbf{J}_0 + \Delta\mathbf{J})^{-1}\Omega(\mathbf{J}_0 + \Delta\mathbf{J})\omega - (\mathbf{J}_0 + \Delta\mathbf{J})^{-1}\mathbf{T}_c - (\mathbf{J}_0 + \Delta\mathbf{J})^{-1}\mathbf{d} + \mathbf{K}_2\omega_e . \tag{24}$$

Considering that the inertia matrix $\mathbf{J}_0 + \Delta\mathbf{J}$ is positive definite and assuming $\frac{d\|\Delta\mathbf{J}\|}{dt}$ negligibly small, the inner loop SMC design is initiated by choosing the candidate Lyapunov function of the form

$$V = \frac{1}{2}s^T(\mathbf{J}_0 + \Delta\mathbf{J})s > 0 . \tag{25}$$

whose derivative is shown as

$$\dot{V} = s^T\left(\frac{1}{2}\Delta\dot{\mathbf{J}}s + (\mathbf{J}_0 + \Delta\mathbf{J})\dot{\omega}_c + (\mathbf{J}_0 + \Delta\mathbf{J})\mathbf{K}_2\omega_e + \Omega(\mathbf{J}_0 + \Delta\mathbf{J})\omega - \mathbf{T}_c - \mathbf{d}\right). \tag{26}$$

To ensure asymptotic stability of the origin of the system eq. (24), the following derivative of the Lyapunov function candidate is enforced[1-4]

$$\dot{V} \le -\eta s^T SIGN(s) = -\eta\sum_{i=1}^{3}|\sigma_i|, \quad \eta > 0 . \tag{27}$$

Further, the sliding surface eq. (23) will reach zero in a finite time[1-4] defined by

$$\tau_r \le \max_{i\in[1,3]}\frac{|s_i(0)|}{\eta}, \tag{28}$$

where $\eta > 0$, and t_r is the design parameter describing the sliding surface reaching time. The value of η is calculated using inequality (28).

Considering inequality (27), the required torque command $\mathbf{T}_c$ to ensure asymptotic stability is defined as

$$\mathbf{T}_c = \mathbf{J}_0\dot{\omega}_c + \mathbf{J}_0\mathbf{K}_2\omega_e + \Omega\mathbf{J}_0\omega + \mu s + \tilde{\rho}SIGN(s). \tag{29}$$

One should note that the SMC eq. (29) is independent of uncertainties $\Delta\mathbf{J}$, $\Delta\dot{\mathbf{J}}$ and disturbances $\mathbf{d}$. Substituting eq. (29) into eq. (26) yields

$$\dot{V} = -\tilde{\rho}\sum_{i=1}^{3}|s_i| - \mu\|s\|^2 + \frac{1}{2}s^T\Delta\dot{\mathbf{J}}s + s^T\left(\Delta\mathbf{J}\dot{\omega}_c + \Delta\mathbf{J}\mathbf{K}_2\omega_e + \Omega\Delta\mathbf{J}\omega - \mathbf{d}\right) \tag{30}$$

Using the inequality[4] $s^T\Delta\dot{\mathbf{J}}s \le \lambda\|s\|^2$, where λ is greater or equal to the maximum eigenvalue of the matrix $\Delta\dot{\mathbf{J}}$, and assuming

$$\left|(\Delta\mathbf{J}\dot{\omega}_c)_i\right| < a_i, \quad \left|(\Delta\mathbf{J}\mathbf{K}_2\omega_e)_i\right| < b_i, \quad \left|(\Omega\Delta\mathbf{J}\omega)_i\right| < c_i, \quad \left|(\mathbf{d})_i\right| < L_i \quad \forall i = \overline{1,3}, \tag{31}$$

then inequality (30) is rewritten as follows:

$$\dot{V} \le -\sum_{i=1}^{3}(\tilde{\rho} - a_i - b_i - c_i - L_i)|s_i| - (\mu - \lambda)\|s\|^2. \tag{32}$$

Inequality (32) is rewritten to enforce inequality (27) after selecting $\mu > \lambda$. This is,

$$\dot{V} \le -\sum_{i=1}^{3}(\tilde{\rho} - a_i - b_i - c_i - L_i)|s_i| \le -\eta\sum_{i=1}^{3}|s_i|. \tag{33}$$

The value of parameter $\tilde{\rho}$ is identified in accordance with inequality (33) as follows:

$$\tilde{\rho} \ge a_i + b_i + c_i + L_i + \eta \tag{34}$$

Remark. The constants $a_i, b_i, c_i, L_i \ \forall i = \overline{1,3}$, are derived by estimating the upper bounds of inequalities (31) within a reasonable flight domain.

To avoid chattering, the SMC eq. (29) is implemented in a continuous form

$$\mathbf{T}_c = \mathbf{J}_0\dot{\omega}_c + \mathbf{J}_0\mathbf{K}_2\omega_e + \Omega\mathbf{J}_0\omega + \mu s + \tilde{\rho}SAT(\Gamma s), \tag{35}$$

where

$$\Gamma = diag\left\{\frac{1}{\zeta_i}\right\}\ \forall i = \overline{1,3},\quad SAT(\Gamma s) = \left\{sat\frac{s_1}{\zeta_1}, sat\frac{s_2}{\zeta_2}, sat\frac{s_3}{\zeta_3}\right\}^T,\quad sat\frac{s_i}{\zeta_i} = \begin{cases} 1, & if\ s_i > \zeta_i \\ \dfrac{s_i}{\zeta_i}, & if\ |s_i| \le \zeta_i \\ -1, & if\ s_i < -\zeta_i \end{cases} \tag{36}$$

Two-loop stability analysis

The outer loop continuous SMC in eqs. (18) and (20) provides global asymptotic stability of the equilibrium point $\sigma = 0$ in accordance with eq. (21). However, the virtual control signal ω_c defined by eqs. (18) and (20) is tracked in the inner loop with a tracking error ω_e. Using backstepping techniques[10], the compensated dynamics of the outer loop sliding surface in eq. (21) must be rewritten as follows

$$\dot{\sigma} = -\rho\mathbf{K}_0\sigma + R(\gamma)\omega_e. \tag{37}$$

Initially, suppose the virtual control signal ω_c is tracked in the inner loop by the discontinuous SMC in eqs. (29) and (34). This SMC provides global asymptotic stability of the equilibrium point $s = 0$, since the negative definiteness of the Lyapunov function derivative in eq. (33) is maintained (given sufficient control power) in the presence of inertia matrix uncertainties and external disturbances. Furthermore, the equilibrium point $s = 0$ is reached in the finite time $t = \tau_r$ in eq. (28). So, $\forall t > \tau_r$ the inner-outer loop compensated dynamics are described as follows:

$$\begin{bmatrix} \dot{\gamma}_e \\ \dot{\sigma} \\ \dot{z} \end{bmatrix} = \begin{bmatrix} -\mathbf{K}_1 - \rho\mathbf{K}_0 & -R(.)\mathbf{K}_2 \\ 0 & -\rho\mathbf{K}_0 & -R(.)\mathbf{K}_2 \\ 0 & 0 & -\mathbf{K}_2 \end{bmatrix} \begin{bmatrix} \gamma_e \\ \sigma \\ z \end{bmatrix}, \qquad \omega_e = -\mathbf{K}_2 z. \tag{38}$$

In accordance with eq. (38) and that matrix $\mathbf{K}_2$ is chosen positive definite, the equilibrium $z = 0$ (and $\omega_e = 0$) is globally asymptotically stable. The equilibrium $\sigma = 0$ is also globally asymptotically stable, since the matrix $\mathbf{K}_0$ is chosen positive definite and $\rho > 0$.

Furthermore, the equilibrium $\gamma_e = 0$ is globally asymptotically stable, since the matrix $\mathbf{K}_1$ is chosen positive definite. Consequently, the system in eq. (38) has a globally asymptotically stable equilibrium $\{\gamma_e, \sigma, z\}^T = 0$.

The γ_e and ω_e error dynamics are de-coupled using the multiple time-scale concept. This is accomplished by selecting positive definite matrices $\mathbf{K}_1$ and $\mathbf{K}_2$ such that $\min\{\mathrm{Re}[eig(\mathbf{K}_2)]\} >> \max\{\mathrm{Re}[eig(\mathbf{K}_1)]\}$, and defining the elements of the diagonal positive definite matrix $\mathbf{K}_0 = diag\left\{\frac{1}{\varepsilon_i}\right\}\ \forall i = \overline{1,3}$ and the scalar $\rho > 0$ such that $\min\{\mathrm{Re}[eig(\rho\mathbf{K}_0)]\} >> \max\{\mathrm{Re}[eig(\mathbf{K}_1)]\}$. This approach causes the $z-$ and $\sigma-$ transients to die out first followed by the $\lim_{t\to\infty} \gamma_e = 0$ according to $\dot{\gamma}_e = -\mathbf{K}_1\gamma_e$.

Now, suppose the virtual control ω_c is tracked in the inner loop by the continuous SMC in eqs. (35) and (36). The derivative of the Lyapunov function in eq. (26) is calculated as follows:

$$\dot{V} \le \begin{cases} -\eta\sum_{i=1}^{3}|s_i|, & if\ |s_i| > \zeta_i \\ -\sum_{i=1}^{3}|s_i|\left(\frac{\rho_i|s_i|}{\zeta_i} - L_i - a_i - b_i - c_i\right), & if\ |s_i| \le \zeta_i \end{cases} \tag{39}$$

The boundary layer $|s_i| = \zeta_i\ \forall i = \overline{1,3}$ will be reached in finite time $t = \tau_r$, since $\dot{V} \le -\eta\sum_{i=1}^{3}|s_i|$ $\forall |s_i| > \zeta_i$[4,5]. The resulting inner-outer loop compensated dynamics, $\forall t > \tau_r$, are described as follows:

$$\begin{bmatrix}\dot{\gamma}_e\\ \dot{\sigma}\\ \dot{z}\\ \dot{s}\end{bmatrix}=\begin{bmatrix}-\mathbf{K}_1-\rho\mathbf{K}_0 & -R(.)\mathbf{K}_2 & R(.)\\ 0 & -\rho\mathbf{K}_0 & -R(.)\mathbf{K}_2 & R(.)\\ 0 & 0 & -\mathbf{K}_2 & \mathbf{I}_{3\times 3}\\ -\mathbf{A}_{41} & -\mathbf{A}_{42} & -\mathbf{A}_{43} & -A_{44}\end{bmatrix}\begin{bmatrix}\gamma_e\\ \sigma\\ z\\ s\end{bmatrix}+\begin{bmatrix}0\\0\\0\\ \mathbf{A}_{45}\end{bmatrix}\mathbf{d}+\begin{bmatrix}0\\0\\0\\ \mathbf{A}_{46}\end{bmatrix}\ddot{\gamma}_r+\begin{bmatrix}0\\0\\0\\ \mathbf{A}_{47}\end{bmatrix}\dot{\gamma}_r \tag{40}$$

where

$$\mathbf{A}_{41}=\left[\left(\mathbf{I}-(\mathbf{I}+\mathbf{E})^{-1}\right)R^{-1}(\gamma)\left(\mathbf{K}_1+\dot{R}(.)R^{-1}(\gamma)\right)-(\mathbf{J}_0+\Delta\mathbf{J})^{-1}\Omega\Delta\mathbf{J}R^{-1}(\gamma)\right]\mathbf{K}_1,$$

$$\mathbf{A}_{42}=\left[\rho\left(\mathbf{I}-(\mathbf{I}+\mathbf{E})^{-1}\right)R^{-1}(\gamma)\left(\mathbf{K}_1+\rho\mathbf{K}_0+\dot{R}(\gamma)R^{-1}(\gamma)\right)-(\mathbf{J}_0+\Delta\mathbf{J})^{-1}\Omega\Delta\mathbf{J}R^{-1}(\gamma)\right]\mathbf{K}_0,$$

$$\mathbf{A}_{43}=\left[\left(\mathbf{I}-(\mathbf{I}+\mathbf{E})^{-1}\right)R^{-1}(\gamma)\left(\mathbf{K}_1+\rho\mathbf{K}_0\right)R(\gamma)+\left(\mathbf{I}-(\mathbf{I}+\mathbf{E})^{-1}\right)\mathbf{K}_2-(\mathbf{J}_0+\Delta\mathbf{J})^{-1}\Omega\Delta\mathbf{J}\right]\mathbf{K}_2,$$

$$\mathbf{A}_{44}=(\mathbf{J}_0+\Delta\mathbf{J})^{-1}(\mu\mathbf{I}+\tilde{\rho}\Gamma)+(\mathbf{J}_0+\Delta\mathbf{J})^{-1}\Omega\Delta\mathbf{J}-\left(\mathbf{I}-(\mathbf{I}+\mathbf{E})^{-1}\right)R^{-1}(\gamma)\left(\mathbf{K}_1+\rho\mathbf{K}_0\right)R(\gamma)-\left(\mathbf{I}-(\mathbf{I}+\mathbf{E})^{-1}\right)\mathbf{K}_2,$$

$$\mathbf{A}_{45}=-(\mathbf{J}_0+\Delta\mathbf{J})^{-1},\quad \mathbf{A}_{46}=\left(\mathbf{I}-(\mathbf{I}+\mathbf{E})^{-1}\right)R^{-1}(\gamma),$$

$$\mathbf{A}_{47}=-\left(\left(\mathbf{I}-(\mathbf{I}+\mathbf{E})^{-1}\right)R^{-1}(\gamma)\dot{R}(\gamma)-(\mathbf{J}_0+\Delta\mathbf{J})^{-1}\Omega\Delta\mathbf{J}\right)R^{-1}(\gamma),\ \mathbf{E}=\mathbf{J}_0\cdot\Delta\mathbf{J}.$$

The first three equations in eqs. (40) are the same as eqs. (38), with the exception of the coupling of the bounded signal s. The system in eq. (38) has a globally asymptotically stable equilibrium $\{\gamma_e,\sigma,z\}^T=0$. Hence, the forced responses described by the first three equations in eqs. (40) are bounded with boundary widths proportional to $\zeta_i\ \forall i=\overline{1,3}$.

In particular, if $\Delta\mathbf{J}=0$, then $\mathbf{A}_{41}=\mathbf{A}_{42}=\mathbf{A}_{43}=\mathbf{A}_{46}=\mathbf{A}_{47}=0$, $\mathbf{A}_{45}=\mathbf{J}_0^{-1}$ and $\mathbf{A}_{44}=\mathbf{J}_0^{-1}(\mu\mathbf{I}+\tilde{\rho}\Gamma)$. Matrix $\mathbf{A}_{44}$ is obviously positive definite and the equilibrium $s=0$ is globally asymptotically stable. Further, if $\lim_{t\to\infty}\mathbf{d}(t)=C=const$, then $\lim_{t\to\infty}s=(\mu\mathbf{I}+\tilde{\rho}\Gamma)^{-1}C=const$ and $\lim_{t\to\infty}z=\mathbf{K}_2^{-1}(\mu\mathbf{I}+\tilde{\rho}\Gamma)^{-1}C=const$. It is easy to show that in this case $\lim_{t\to\infty}\sigma=\lim_{t\to\infty}\gamma_e=0$.

The following are conclusions derived from the two-loop stability analysis of the continuous inner and outer loop SMCs operating in the presence of bounded inertia $\Delta\mathbf{J}$ and external torque $\mathbf{d}$ disturbances:

- The asymptotic transient behavior of the inner and outer loop tracking errors γ_e and ω_e, which are controlled by the continuous outer loop SMC and the discontinuous inner loop SMC, are de-coupled in presence of bounded $\Delta\mathbf{J}$ and external disturbance torque $\mathbf{d}$.
- The tracking errors γ_e and ω_e, which are controlled by the continuous outer loop SMC and the continuous inner loop SMC, are bounded in presence of bounded $\Delta\mathbf{J}$ and external disturbance torque $\mathbf{d}$.
- The asymptotic transient behavior of the inner and outer loop tracking errors γ_e and ω_e, which are controlled by the continuous outer loop SMC and the continuous inner loop SMC, are de-coupled in presence of external disturbance torque $\mathbf{d}$: $\lim_{t\to\infty}\mathbf{d}(t) = C = const$ and completely known matrix of inertia $\mathbf{J}$.

Control Allocation

The command torque $\mathbf{T}_c$ is related to the deflection command vector $\delta_c \in \mathbf{R}^n$ as follows:

$$\mathbf{T}_c = \mathbf{D}(.)\delta_c . \tag{41}$$

Assuming $rank\mathbf{D}(.) = rank[\mathbf{D}(.), \mathbf{T}_c] = 3$, it is obvious that given a $\mathbf{T}_c$ profile, there exist an infinite number of corresponding δ_c profiles that satisfy eq. (41). This lends itself to the following optimization problem

$$\min_{\delta_c \in \Pi} \mathrm{f}(\delta_c) = \delta_c^T \mathbf{Q} \delta_c ,\ \Pi\text{: } \{\delta_c | \mathbf{D}(.)\delta_c - \mathbf{T}_c = 0\}, \tag{42}$$

which is minimized by the solution

$$\delta_c = \mathbf{Q}^{-1}\mathbf{D}(.)^{\mathrm{T}}\left[\mathbf{D}(.)\mathbf{Q}^{-1}\mathbf{D}(.)^{\mathrm{T}}\right]^{-1}\mathbf{T}_c \ . \tag{43}$$

Eq. (43) is re-written as

$$\delta_c = \mathbf{B}_v\mathbf{T}_c \ , \tag{44}$$

where

$$\mathbf{B}_v = \mathbf{Q}^{-1}\mathbf{D}(.)^{\mathrm{T}}\left[\mathbf{D}(.)\mathbf{Q}^{-1}\mathbf{D}(.)^{\mathrm{T}}\right]^{-1} \tag{45}$$

is the control allocation (gain-mixing) matrix, $\mathbf{Q}$ is the weighting matrix, and $\mathbf{D}(.)$ is the torque-to-deflection partial derivative matrix or sensitivity matrix.

Design and Simulation of the X-33 RLV Control System in the Launch Mode

The X-33 technology demonstration RLV controller design is considered in the launch mode. The 6DOF high fidelity mathematical model includes the control deflection vector $\delta \in \mathbf{R}^{11}$ that consists of the following components: δ_1 and δ_2 are deflections of the right and left flaps (in radians); δ_3 and δ_4 are deflections of the right and left inward elevons (in radians); δ_5 and δ_6 are deflections of the right and left outward elevons (in radians); δ_7 and δ_8 are deflections of the right and left rudders (in radians); δ_9, δ_{10}, and δ_{11} are pitch, roll and yaw differential throttles (in % of power level) of the aerospike rocket engine. Flight guidance tables for the Euler angle command profiles γ_c are used. High fidelity sensor mathematical models with 0.02 s time delay as well as realistic table look up wind gust profiles that create a disturbance torque are also used.

The command profiles ω_c and $\mathbf{T}_c$ are generated by the outer and inner loop SMCs in eqs. (18), (20) and (35). The deflection command vector δ_c is calculated in eq. (9) and executed by the actuators, whose dynamics are contained in high fidelity models used in the simulations.

In the calculation of the control allocation matrix $\mathbf{B}_v$ in eq. (45), the $\mathbf{Q}^{-1}$ matrix is chosen to be diagonal. The diagonal terms are equal to square maximum deflections $\delta_{i\max}^2$, which provide both a dimensionless performance index $f(\delta_c) = \delta_c^T \mathbf{Q} \delta_c$ and a uniform penalty function for each command δ_c. The control torque $\mathbf{T}$ is calculated by eq. (8) and used in eq. (1) during the simulation. The time-varying sensitivity matrix $\mathbf{D}(.)$ is obtained by linearizing through the aerodynamic and propulsion system data bases at various flight conditions.

The outer loop continuous SMC is designed in accordance with eqs. (12), (18) and (20). The following outer loop SMC parameters are chosen:

$$\rho = 1,\ \mathbf{K}_0 = \begin{bmatrix} 1.0 & 0 & 0 \\ 0 & 0.8 & 0 \\ 0 & 0 & 1.5 \end{bmatrix},\ \mathbf{K}_1 = \begin{bmatrix} 0.4 & 0 & 0 \\ 0 & 0.4 & 0 \\ 0 & 0 & 0.4 \end{bmatrix}, \tag{46}$$

where the matrix $\mathbf{K}_1$ provides a $0.4\,rad/s$ given bandwidth for the compensated outer loop. The inner loop continuous SMC is designed in accordance with eqs. (23), (34) and (35). The following inner loop SMC parameters are chosen:

$$\hat{\rho} = \begin{bmatrix} 3.8\cdot 10^6 & 0 & 0 \\ 0 & 3.8\cdot 10^6 & 0 \\ 0 & 0 & 5.0\cdot 10^6 \end{bmatrix} N\cdot m,\ \mathbf{K}_2 = \begin{bmatrix} 1.88 & 0 & 0 \\ 0 & 1.88 & 0 \\ 0 & 0 & 1.88 \end{bmatrix}, \tag{47}$$

where the matrix $\mathbf{K}_2$ provides a $1.88\,rad/\sec$ given bandwidth for the compensated inner loop, and $\mu = 0$ is chosen since the matrix $\Delta\dot{\mathbf{J}}_0$ is a negative definite.

The 6DOF time simulation results are presented in figures 1 - 18. Figures 1 - 3 and figure 7 show overall tracking performance of the Euler angle guidance profiles in the outer loop, which is obviously decoupled and very accurate. Figures 4-6 show reasonably accurate tracking the angular rates command profiles in the inner loop. Figures 14 and 15 demonstrate torque

command profiles $\mathbf{T}_c$. These commands are allocated into actuator deflection commands δ_c and executed by the actuators. Figures 8-13 demonstrate corresponding deflections of the aerodynamic surfaces and engine differential throttles that are far from saturation. Figures 16-18 show that tracking motion happens in the close vicinities of the sliding surfaces. This means that the robust accurate real sliding mode exists in the X-33 control system by means of the two loop multiple scale SMC in the presence of wind disturbances and inertia uncertainties.

Conclusions

Employing a time scaling concept in the inner (angular rates) and outer (orientation angles) loops, a new two-loop continuous SMC was designed for the RLV. This SMC provides de-coupled performance in the inner and outer loops in presence of bounded external disturbances and plant uncertainties. Stability of the two-loop control system is analyzed. A control allocation matrix is designed that optimally distributes the roll, pitch, and yaw torque commands into end-effector deflection commands. 6 DOF high fidelity simulation show that the multiple scale SMC provides robust, accurate, de-coupled tracking of the commanded Euler angle guidance profiles for the X-33 RLV in the ascent mode in the presence of external disturbances (wind gusts) and plant uncertainties (changing matrix of inertia).

References

[1]DeCarlo, R. A., Zak, S. H., and Matthews, G. P. "Variable structure control of nonlinear multivariable systems: a tutorial," *IEEE Proceedings*, **76**, pp. 212-232. 1988.

[2]Utkin, V. I., *Sliding Modes in Control and Optimization*, Berlin, Springer - Verlag, 1992.

[3]Hung, J. Y., Gao, W., and Hung, J. C., "Variable Structure Control: A Survey," *IEEE Transactions on Industrial Electronics,* **40**, 1, pp. 2-21, 1993.

[4]Slotine, J-J., and Li, W., *Applied Nonlinear Control,* Prentice Hall, New Jersey, 1991.

[5]Esfandiari, F., and Khalil, H.K., "Stability Analysis of a Continuous Implementation of Variable Structure Control," *IEEE Transactions on Automatic Control*, **16**, 5, pp. 616-619, 1991.

[6]Shtessel, Y., and Buffington, J., "Finite-reaching-time continuous sliding mode controller for MIMO nonlinear systems," *Proceedings of the 37th CDC*, Tampa, FL, 1998, pp. 1934-1935.

[7]Dwyer, T. A. W., III, and Sira-Ramirez, H., "Variable Structure Control of Spacecraft Attitude Maneuvers," *Journal of Guidance, Control and Dynamics*, **11**, 3, pp. 262-270, 1988.

[8]Naidu, D. S., and Calise A. J., "Singular Perturbations and Time Scales in Guidance, Navigation, and Control of Aerospace Systems: Survey," *Proceedings of the AIAA Guidance, Navigation, and Control Conference,* Baltimore, MD, August 1995, pp. 1338-1362.

[9]Shtessel, Y., McDuffie, J., Jackson, M., Hall, C., Krupp, D., Gallaher, M., and Hendrix, N. D., "Sliding Mode Control of the X-33 Vehicle in Launch and Re-entry Modes," *Proceedings of the AIAA Guidance, Navigation, and Control Conference,* August 1998, pp.1352-1362.

[10]Krstic, M., Kanellakopoulus, I., and Kokotovic, P. *Nonlinear and Adaptive Control Design,* John Wiley and Sons, NY, 1995.

[11]Azam, M., and Singh, S., "Invertibility and Trajectory Control for Nonlinear Maneuvers of Aircraft," *Journal of Guidance, Control, and Dynamic*, **17**, 1, pp. 192-200, 1994.

List of captions

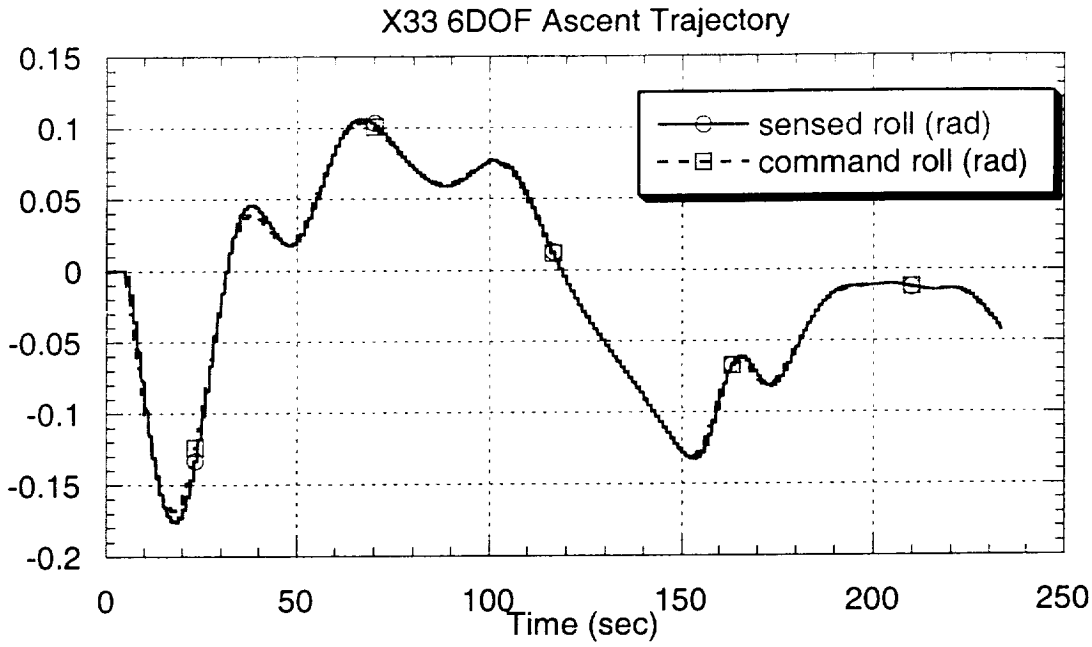

Figure1 Roll profile tracking

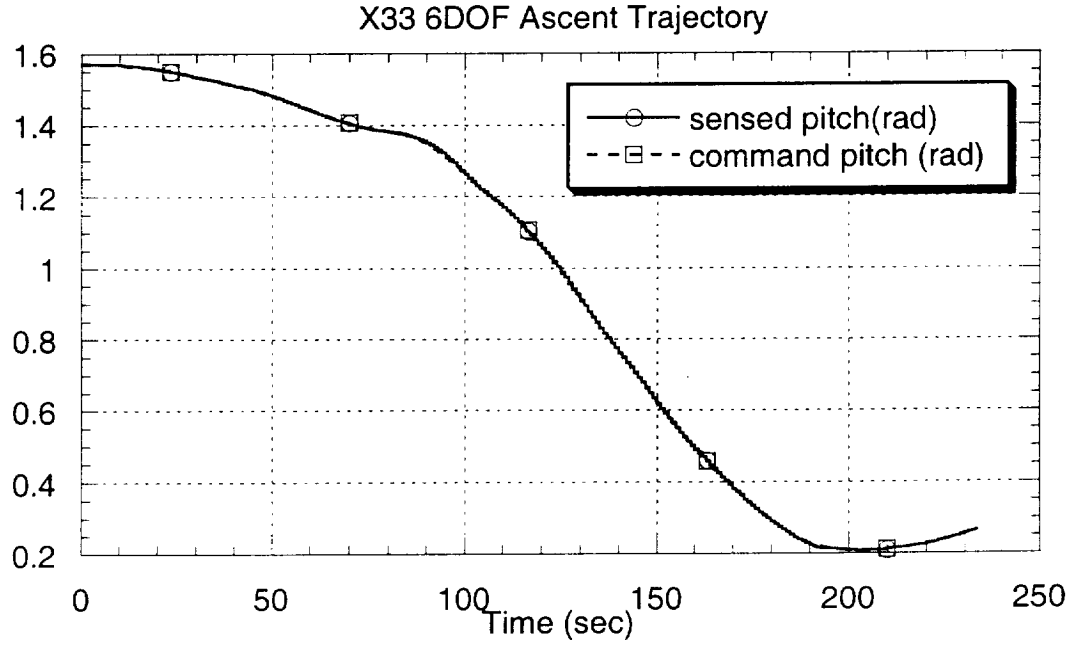

Figure 2 Pitch profile tracking

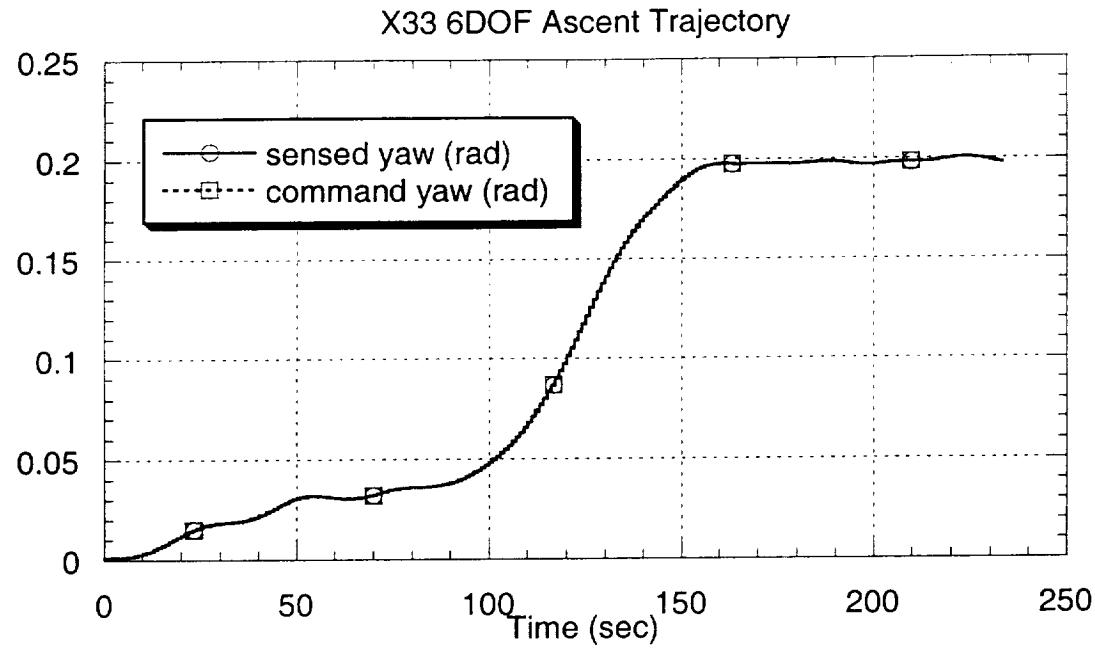

Figure 3 Yaw profile tracking

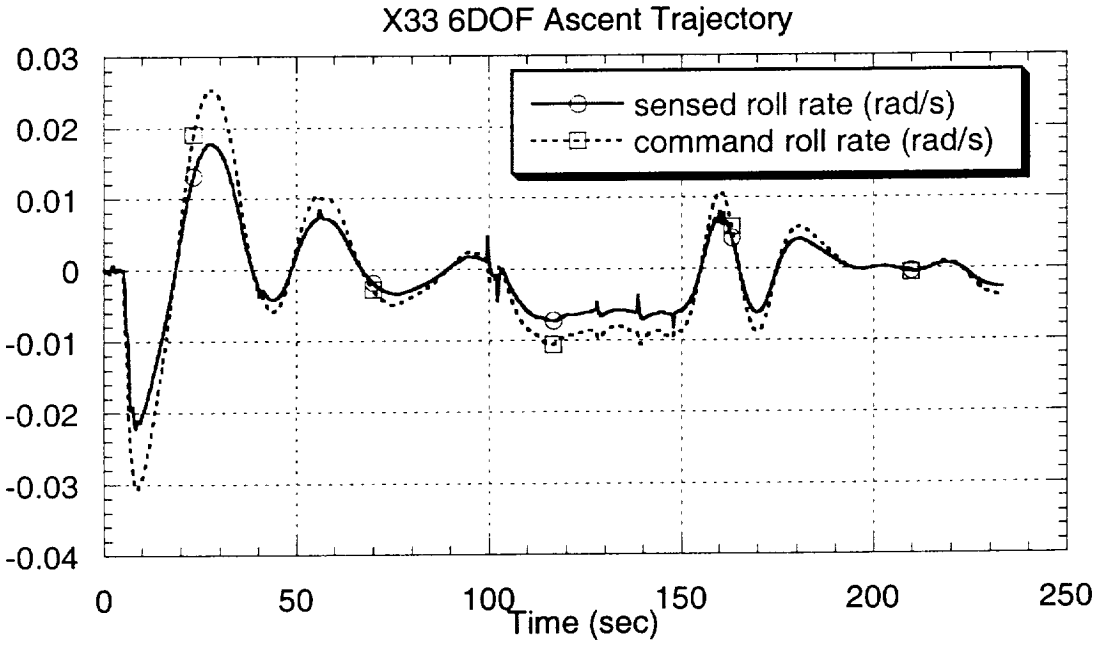

Figure 4 Roll rate command tracking

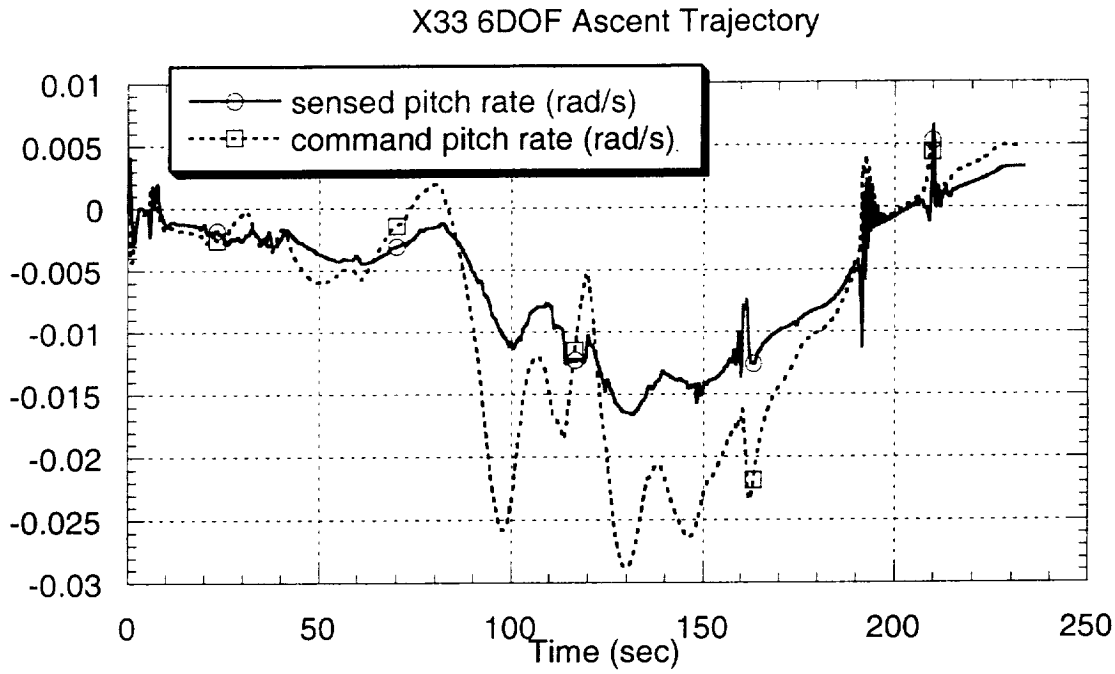

Figure 5 Pitch rate command tracking

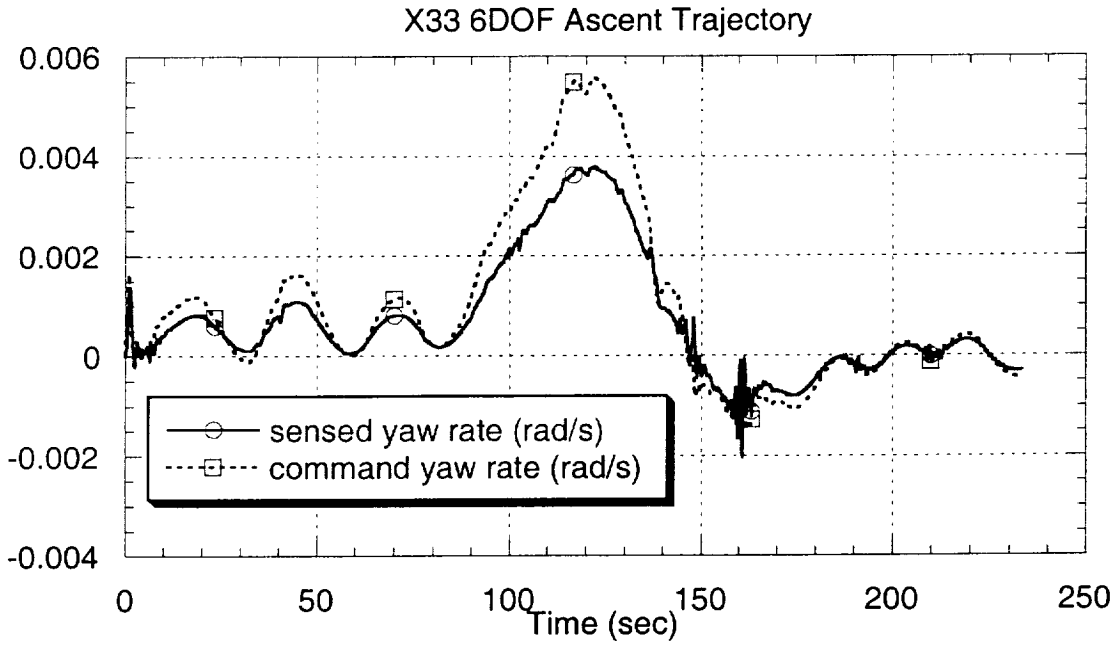

Figure 6 Yaw rate command tracking

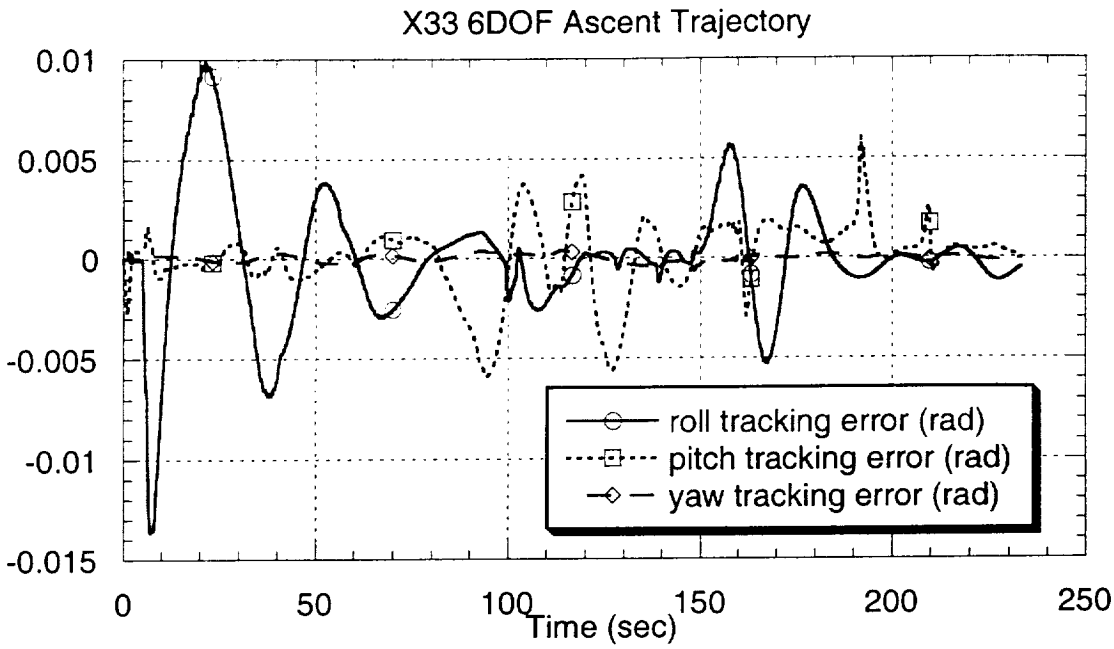

Figure 7 Orientation angle tracking errors

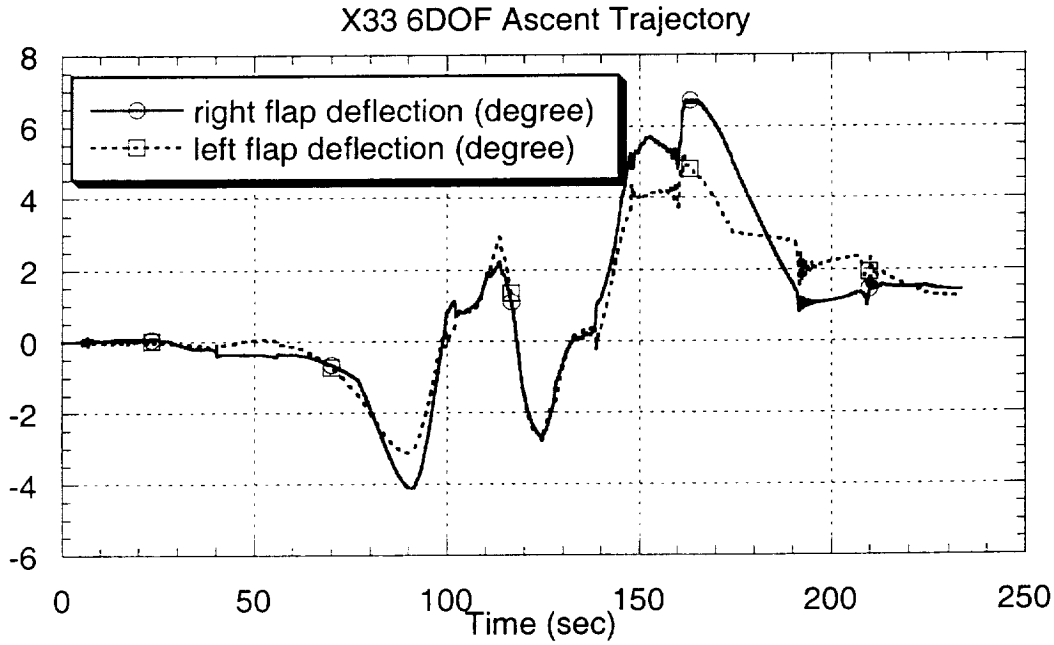

Figure 8 Flap deflections

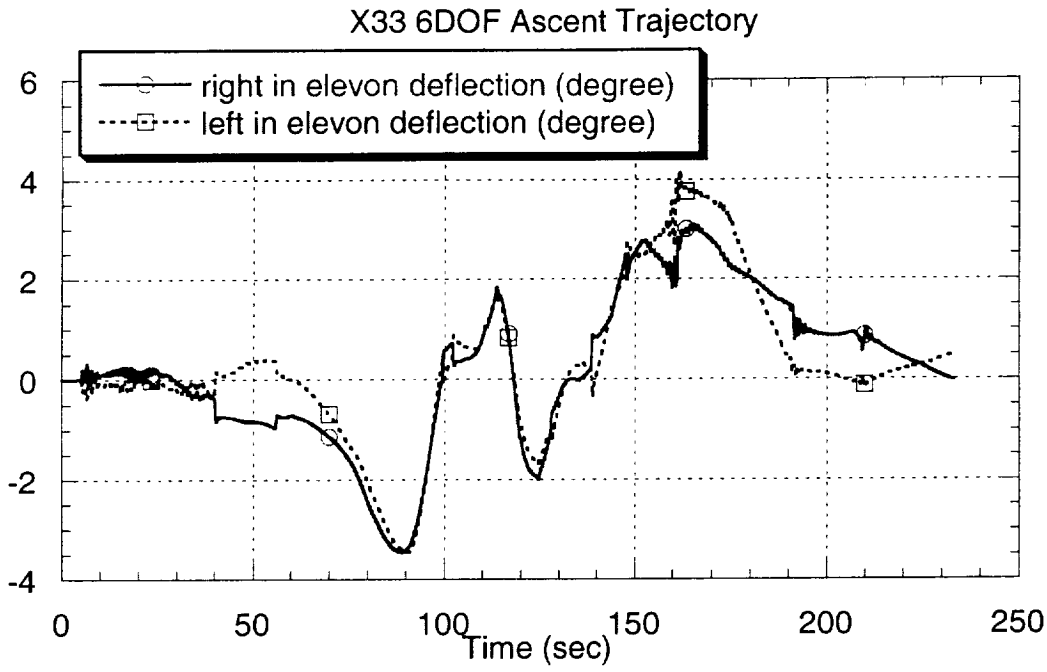

Figure 9 Inward elevon deflections

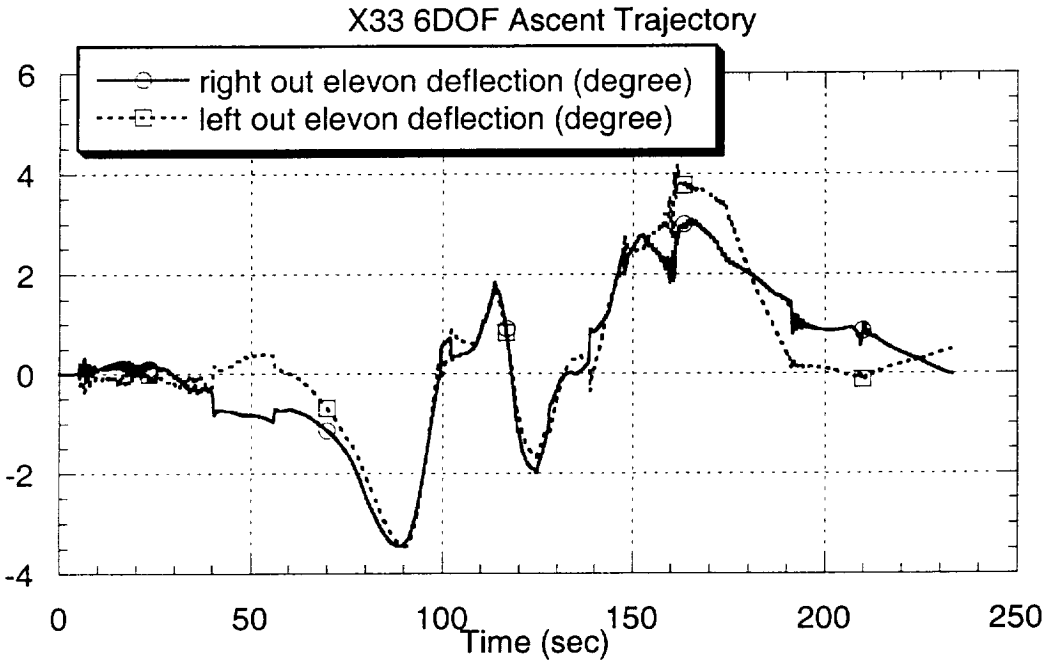

Figure 10 Outward elevon deflections

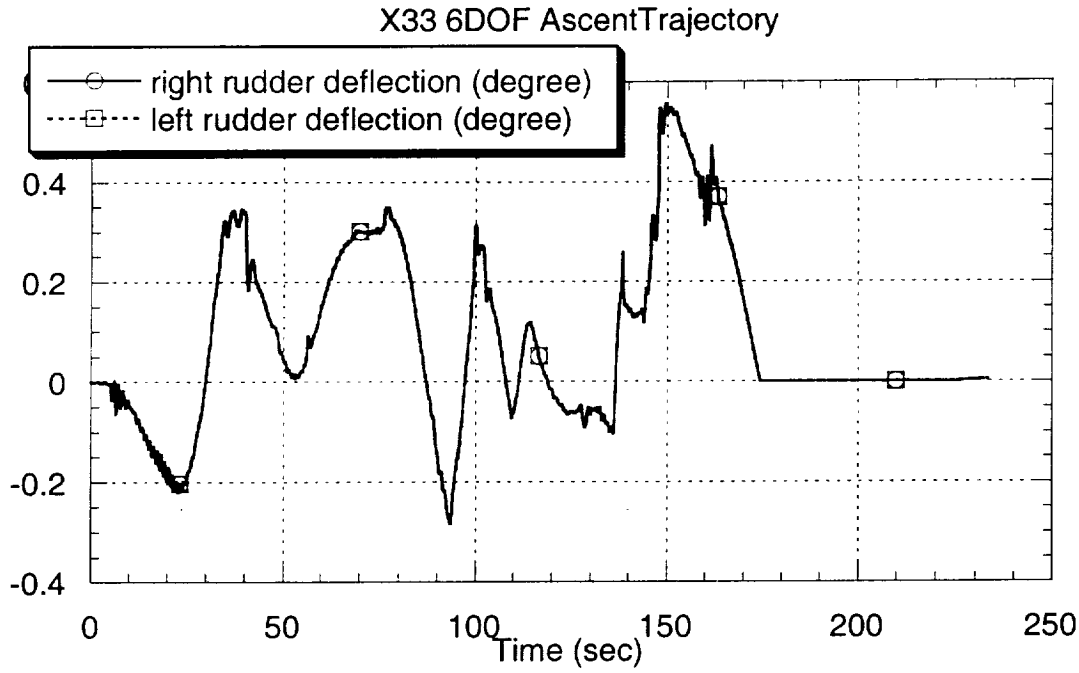

Figure 11 Rudder deflections

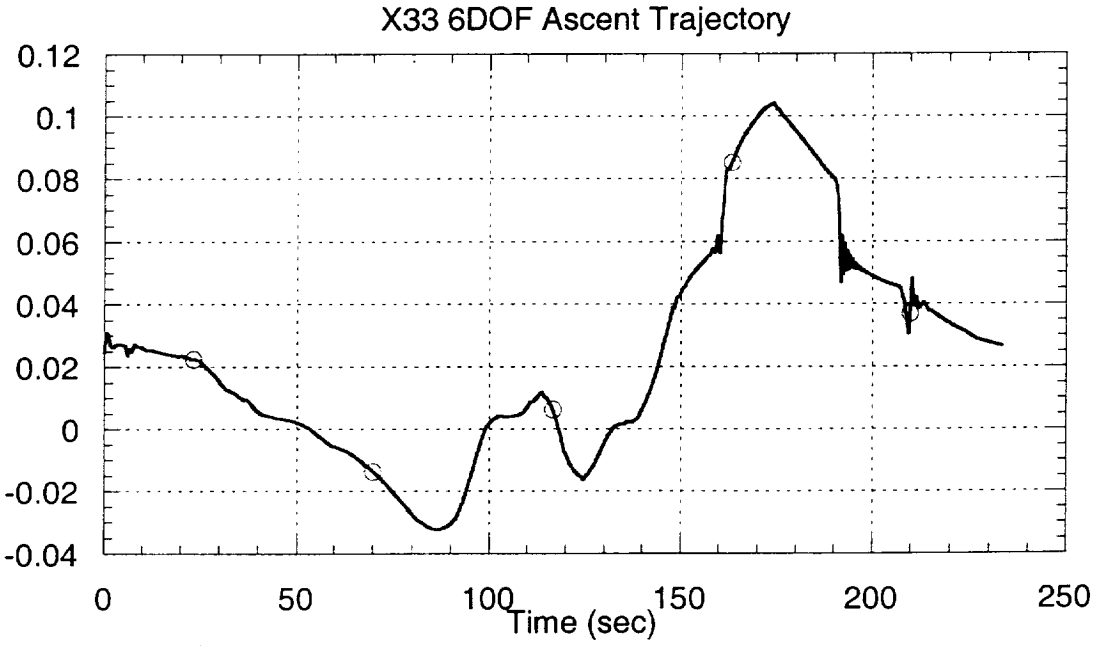

Figure 12 Pitch differential throttle

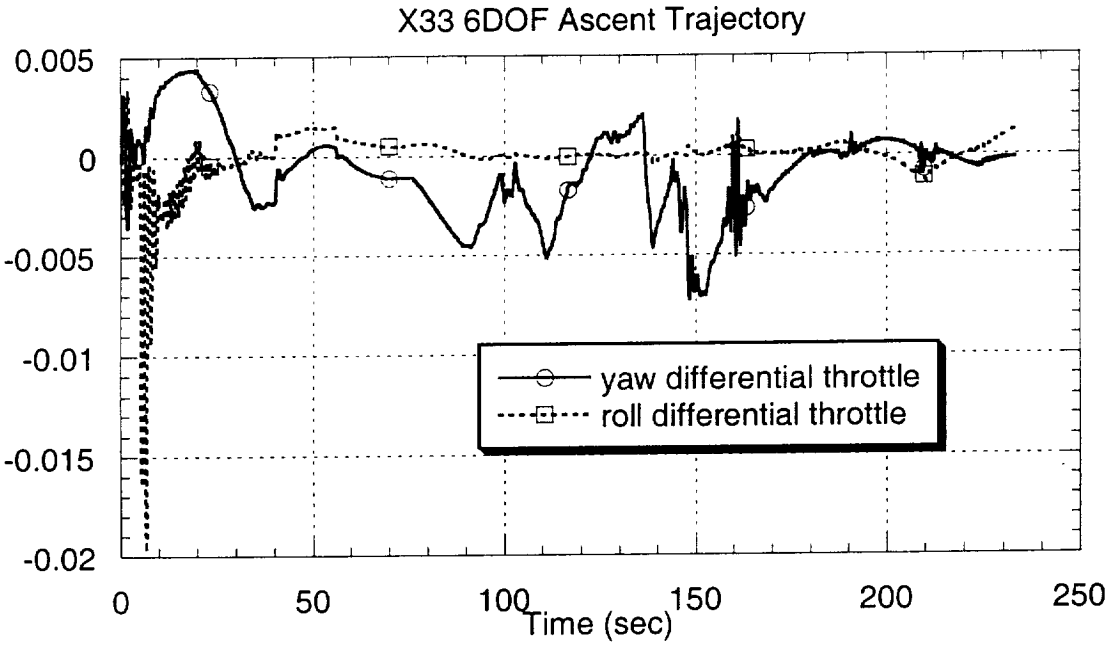

Figure 13 Roll and Yaw differential throttle

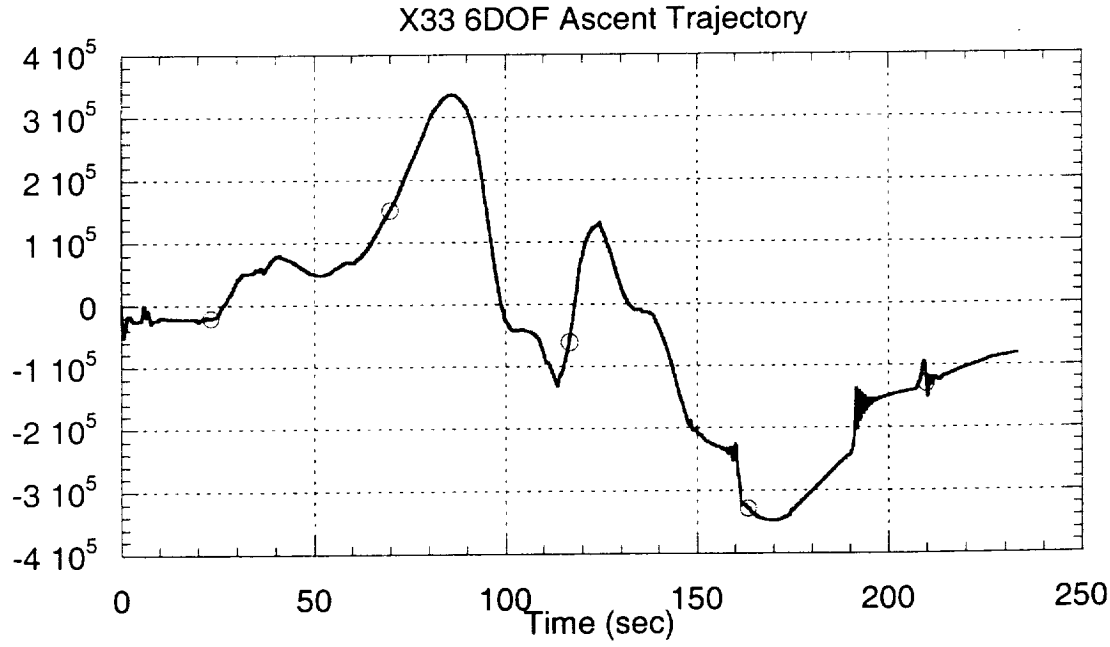

Figure 14 Pitch command torque (lb-ft)

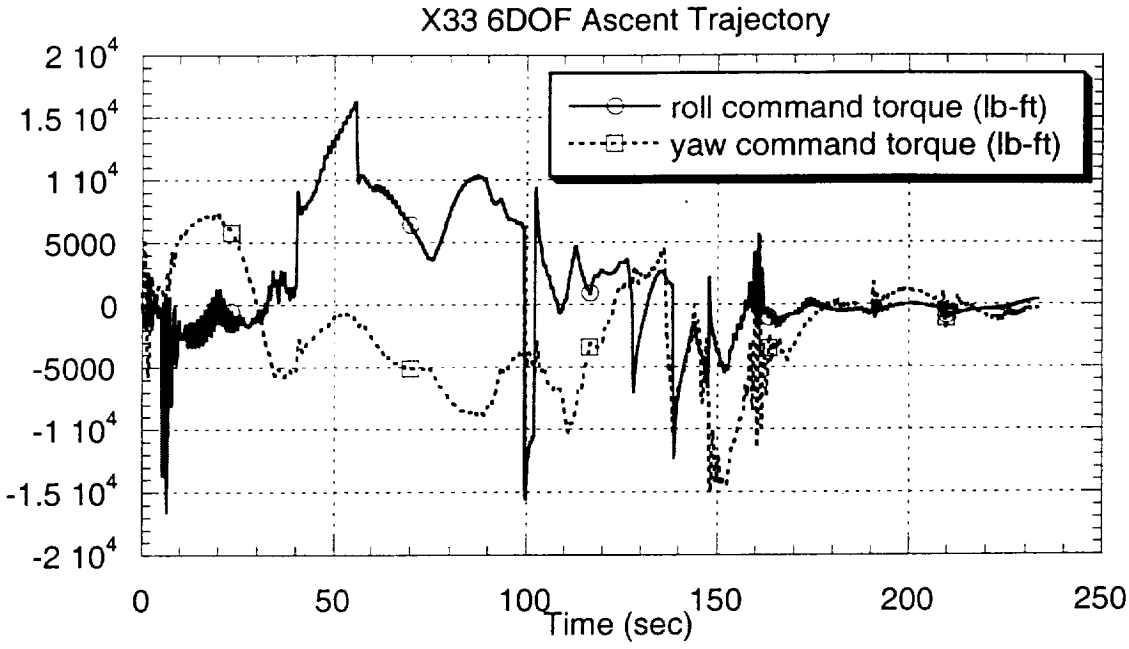

Figure 15 Roll and Yaw command torque

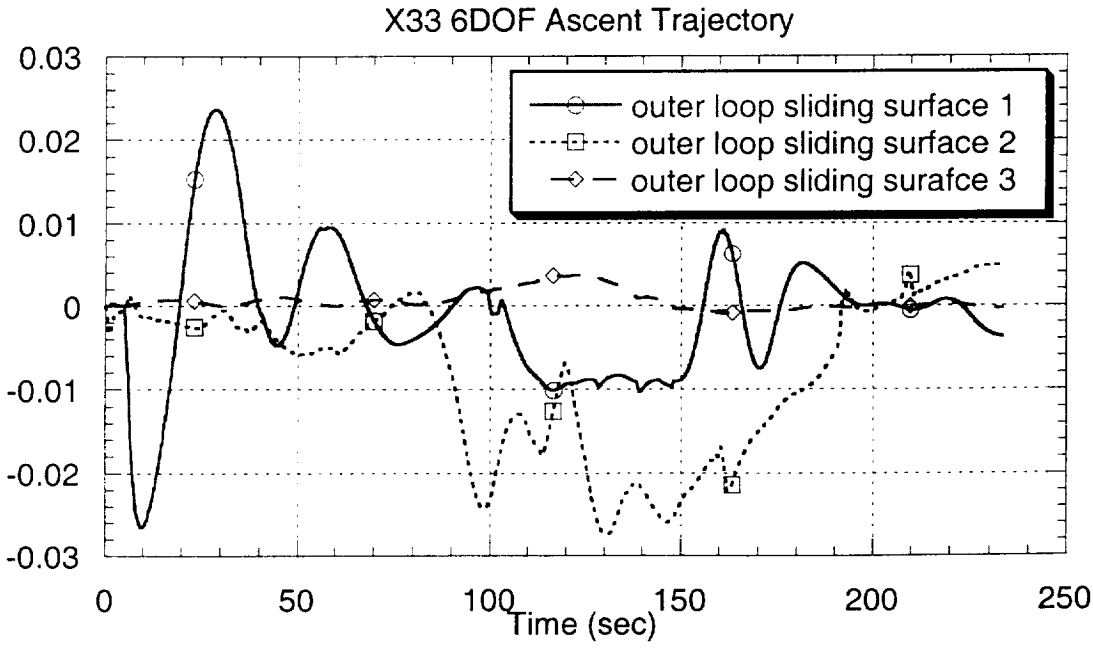

Figure 16 Outer loop sliding surfaces

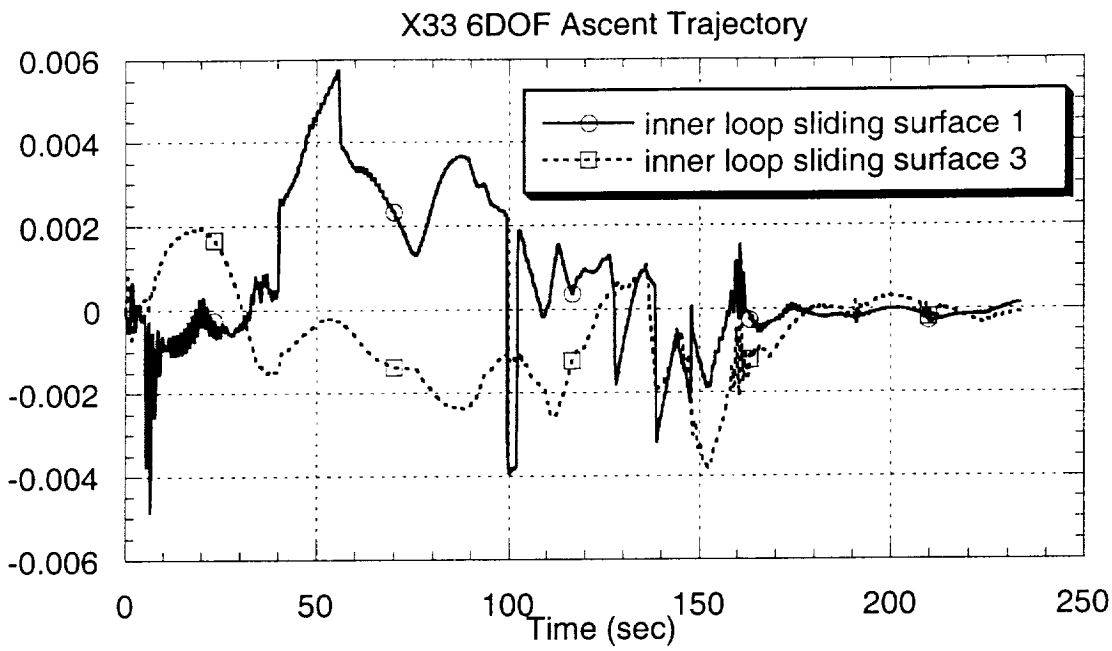

Figure 17 Inner loop sliding surfaces 1 and 3

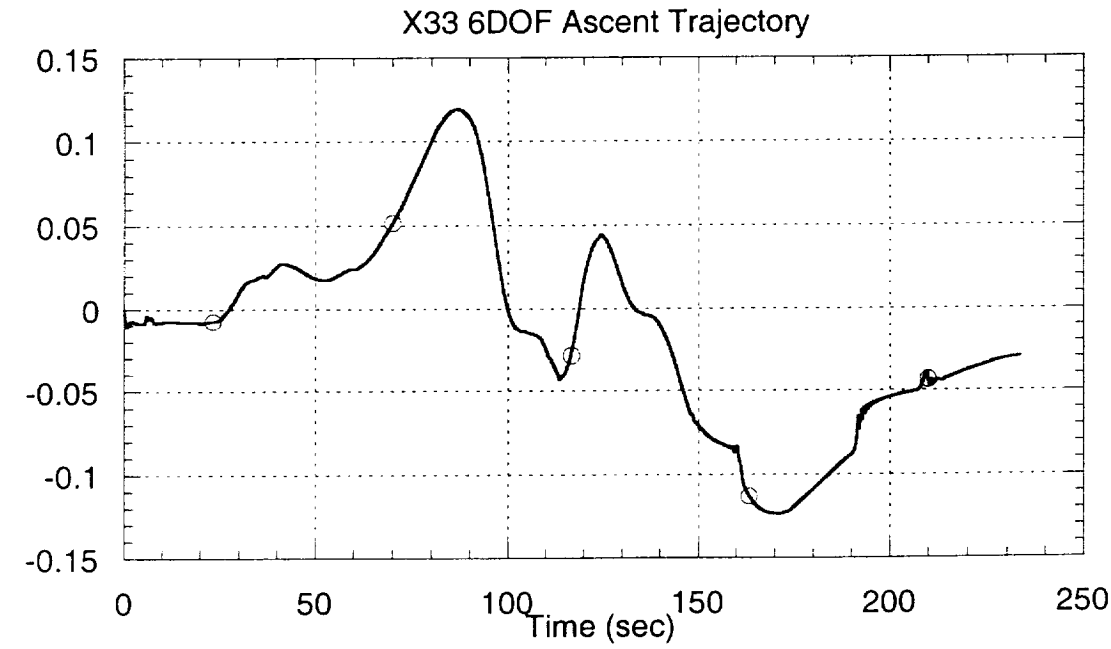

Figure 18 Inner loop sliding surface 2